Journal of Colloid and Interface Science 348 (2010) 152–158

Contents lists available at ScienceDirect

Journal of Colloid and Interface Science

www.elsevier.com/locate/jcis

A rheological study in the dilute regime of the worm-micelle fluid made of zwitterionic surfactant (TDPS), anionic surfactant (SDS), and brine

David Lopez-Diaz, Erick Sarmiento-Gomez, Cristina Garza, Rolando Castillo *

Instituto de Física, Universidad Nacional Autónoma de México, P. O. Box 20-364, Mexico D.F. 01000, Mexico

ARTICLE INFO

Article history:
Received 21 January 2010
Accepted 17 March 2010
Available online 21 March 2010

Keywords:
Wormlike micelles
Shear thickening
Zwitterionic surfactant
Sulfobetaine

ABSTRACT

We present a rheological study for a system made of zwitterionic surfactant N-tetradecyl-N,N-dimethyl-3-ammonio-1-propanesulfonate (TDPS), sodium dodecyl sulfate (SDS), and water (0.5 M NaCl). We found that this system forms wormlike micelles. This study is focused in the dilute regime below the overlap concentration, where micelles are not entangled. The overlap concentration was determined using dynamic light scattering. The behavior of the apparent viscosity and the shear stress, both as a function of the shear rate, was determined for different zwitterionic surfactant concentrations, temperatures, and two surfactant ratios ($R = [SDS]/[TDPS]$). The shear-thickening transition and its temperature dependence was also studied. Finally, we were able to observe the shear-induced structures by using the scattered light from a sheet of light perpendicular to the flow that is installed in the gap of a transparent Couette cell filled with the micellar fluid.

1. Introduction

Blends of zwitterionic and anionic surfactants often exhibit significant synergism (strong favorable interactions) in aqueous solutions. Therefore, it would not be peculiar that they spontaneously self-assemble into long and flexible cylindrical micelles, transforming micellar solutions into viscoelastic fluids. Typical examples of mixtures of anionic and zwitterionic surfactants, involve betaines and sulfobetaines. Betaines have shown a strong synergism when mixed with sodium dodecyl sulfate (SDS), clearly exemplified by the critical micelar concentration (CMC) dependence on composition [1]. In sulfobetaines, where charge is not sensitive to pH, one can find examples in aqueous solution where the interaction between zwitterionic surfactants and SDS is not important. However, the addition of an inert electrolyte to the solution, clearly favors the interaction [2]. This is the case of the mixture of N-tetradecyl-N,N-dimethyl-3-ammonio-1-propanesulfonate (TDPS) and SDS, in brine. As will become clear in the present study, this interaction promotes the self-assembly of these surfactants into long and flexible cylindrical micelles, i.e., in worm-micelles (WMs), making the system made of TDPS/SDS/water (0.5 M NaCl) interesting for structural and rheological studies. As far as we know, it has not been reported the ability of this system to form WMs.

Micelles are the result of equilibrium self-assembly. Their size distribution reflects a free-energy minimum that may vary with concentration. WMs impart the micellar fluid solutions a strong non-linear response under imposed flow fields. Some reviews have summarized several decades of intense research [3–5]. Above the overlap concentration, C^*, defining the boundary between dilute and semidilute regimes, micelles are entangled. Here, WM solutions show quite intriguing properties [6]. Just to mention the most fascinating ones [4–6]: Maxwellian behavior, non-linear rheological behavior with a plateau in the shear stress (σ) vs shear rate ($\dot{\gamma}$) flow curve, and shear banding. Below C^*, but above the critical micellar concentration, the long micelles are on average not overlapping. Notwithstanding the low surfactant concentration, the micellar fluid can present a strong non-linear response under imposed flow fields and properties like shear thickening and rheopexy. Although, many features change from one system to another, dilute WM solutions have characteristics in common. In most of them, when shear rate is imposed, curves of apparent viscosity vs shear rate present shear thickening above a critical shear rate, $\dot{\gamma}_c$. After reaching a maximum, where apparent viscosity is raised by a factor of 2–50, the system shear thins at higher shear rates; before this $\dot{\gamma}_c$ the system is Newtonian or slightly thinning [7,8]. Typically, $\dot{\gamma}_c$ increases with concentration as a power law [9,10], although this is not general [11]. After a sudden application of a constant shear rate larger than $\dot{\gamma}_c$, there is usually an induction period, τ_{ind}, where shear stress begins to increase sharply up to a steady-flow plateau; $\tau_{\mathrm{ind}} \sim 1/\dot{\gamma}_c$ [10]. The higher the temperature, T, the longer the induction period [10]. With added salt, as concentration increases τ_{ind} and $\dot{\gamma}_c$ increases [16]. Shear thickening also decreases with temperature [9]. $\dot{\gamma}_c$ presents an Arrhenius temperature dependence [7–9,12,13], i.e., $\dot{\gamma}_c(\varphi, T) \sim \exp[-E_a/k_BT]$, where E_a is an activation energy and k_B is the Boltzmann's constant. Shear thickening is often difficult to study because it could be history dependent [14,15]. WM solutions present flow birefringence showing that the development of a highly aligned

* Corresponding author. Fax: +52 55 561 61535.
E-mail address: rolandoc@fisica.unam.mx (R. Castillo).

0021-9797/$ - see front matter © 2010 Published by Elsevier Inc.
doi:10.1016/j.jcis.2010.03.038

phase approximately coincides with the shear-thickening transition [17]. However, it has been suggested that micelle growth occurs already at shear rates smaller than $\dot{\gamma}_c$, and that the shear thickening occurs once the mean size of the aggregates has reached some critical value [18]. Small-angle neutron scattering (SANS) studies strongly suggest that the increase in viscosity observed above $\dot{\gamma}_c$ is associated with a shear-induced growth of the micellar aggregates [19]. In addition, SANS scattering data under shear [9] have established a correlation between flow and structure. In the thickening region, SANS patterns were interpreted as the superposition of two coexisting states, one viscoelastic entangled sheared network and one still purely viscous made of short aggregates. At larger $\dot{\gamma}$, the former state dominates and its increasing orientation results in shear-thinning. SANS data also have shown that structures induced by shear remain for a long time after the cessation of the shear [19]. However, if the shear rate is removed during the induction period, the stress vanishes to zero instantaneously [10]. Light scattering experiments [7,20,21] suggest that the shear thickening effect is a shear-induced gelation followed by a fracture of the gel [17]. The sheared–induced gel-like and oriented phase is made of shear-induced structures (SIS) forming large fluctuating domains that coexist with a homogeneous fluid phase containing unstructured aggregates [22]. The portion of the fluid with SIS increases with shear rate [22,23]. In particular, small angle light scattering has shown the emergence of long rod-like structures along the flow direction, which start to form at the shear-thickening transition [7]. No appreciable spacing correlation between them was observed along the flow direction, indicating that the rod-like structures may be long micellar bundles forming entangling fibers [7].

This is the first paper of a series relating the micellar solution structure to its rheological behavior, for the TDPS/SDS/brine system. The first aim of the paper will be to present some tests to infer the nature of the self-assembled supramolecular structures in the system above C^* (results are more clearly observed there), such as, evidence of flow birefringence and of Maxwellian behavior in the viscoelastic spectra, as well as evidence of an entangled network of long flexible tubular objects obtained by transmission electron microscopy (TEM). These tests led to a new finding, namely, that the system under study self-assembles into long and flexible cylindrical micelles. The second aim is to understand the rheological behavior of the system in the dilute regime (below C^*). It presents specific characteristics to be contrasted with other well-known WM solutions. Here, we will assume that on dilution, i.e., below C^*, as in other WM solutions the system is still formed by non-entangled WMs, which are responsible for the singular rheological behavior to be illustrated below. C^* was estimated by using dynamic light scattering (DLS) intensity correlation functions. Collective diffusion coefficients (D) as a function of the zwitterionic surfactant concentration (C_z) were also obtained. The minima in these graphs agree with the C^* values estimated by DLS. The behavior of the apparent viscosity (η) and of the shear stress (σ) was determined, both as a function of the shear rate ($\dot{\gamma}$) for different C_z and T, at two surfactant ratios (R = *[SDS]/[TDPS]*). We found that $\dot{\gamma}_c$ follows Arrhenius' law and activation energies were obtained. Finally, we were able to observe shear-induced structures (SIS) in this system, with the aid of light scattering. Our findings provide a new insight of the structure and the rhological properties of this system.

2. Experimental section

2.1. Materials

N-tetradecyl-N,N-dimethyl-3-ammonio-1-propanesulfonate (TDPS, >99%) and sodium chloride (>99%) were from Sigma–Aldrich (USA), and sodium dodecyl sulfate (SDS, >99%) from Merck (Germany). All the reagents were used as received. Water was Milli-Q water (nanopure-UV, USA; 18.3 MΩ). All micellar solutions were prepared by weight, varying C_z at two different surfactant ratios (R = *[SDS]/[TDPS]*): 0.45 and 0.55 in water at 0.5 M in NaCl. Measurements were made at least two days after the solution preparation to allow them to reach equilibrium.

2.2. Rheology

Rheometric measurements were performed on a Bohlin Gemini HRnano rheometer (Malvern Instruments, UK). Most of the rheometric measurements were done using the same cone-plate geometry (4°–40 mm). When other geometries were used, the shape of the flow curves, as well as the stress values were essentially the same. Optical rheometric observations were performed in a homemade transparent Couette rheometer [22]. This transparent Couette rheometer is made of two concentric quartz cylinders (50 mm height). The inner cylinder (O.D. 75 mm) is fixed and filled with water coming from a thermal regulated circulatory bath for thermal control. The external cylinder (O.D. 85 mm) rotates over air bearings; shear mode can be used with the aid of a dc-motor. The gap between cylinders is 2.5 mm wide. A section of the gap with the fluid can be visualized using a zoom lens combination focused at a sheet of light perpendicular to the flow velocity that is obtained with a He–Ne laser beam and a combination of spherical and cylindrical lenses. The zoom lens is mounted on a video camera.

2.3. DLS

The experimental set up is a homemade apparatus. Laser light comes from a Spectra-Physics laser (Spectra Physics, CA) that illuminates the sample, which is in a thermal bath with temperature control of ±0.2 °C (Cole-Parmer, USA). Dispersed light is detected with a THORN EMI photomultiplier (THORN-EMI, UK) coupled to a ALV preamplifier, and to an ALV-5000/E multiple tau digital correlator (ALV Langen, Germany) to get the intensity autocorrelation function, $g^{(2)}(q,t)$. $q = (4\pi n/\lambda_0)\sin(\theta/2)$. Here, q is the magnitude of the scattering vector, n is the refractive index of the solution, λ_0 is the laser wavelength in vacuum, and θ is the scattering angle. The measured intensity autocorrelation function is converted into the electric field autocorrelation function, $g^{(1)}(q,t)$, using the Siegert relationship: $|g^{(2)}(q,\tau)| = 1 + \beta|g^{(1)}(q,\tau)|^2$, where β is a constant that depends on the scattering geometry. Relaxation times are obtained using CONTIN-ALV software. DLS experiments were performed on micellar solutions at several angles (55°, 65°, 70°, 85°, 90°, 95°, 105°, 115°, 125°, and 130°). A regularized inverse transformation algorithm, incorporated in the ALV/5000/E program, was performed on $g^{(1)}(q,t)$ functions. In this way, relaxation times (τ_{rel}) or decay rates, $\Gamma = Dq^2 = \tau_{rel}^{-1}$, were obtained from the relaxation time distribution peaks. Collective diffusion coefficients were obtained from the slope of Γ versus q^2.

2.4. High angle annular dark field (HAADF) TEM micrographs

A sample of the micellar solution was applied to a carbon-coated TEM grid, and most of the solution was removed by blotting with the edge of a filter paper. Afterward, a solution made of 2% uranyl acetate for negative staining was applied, and the sample was dried again. HAADF was employed for the microstructural analysis of the sample, which was performed in a TEM JEM-2010F FASTEM with an ultimate resolution point to point of 1.9 Å fitted with a Gatan Image Filter.

3. Results and discussion

3.1. Wormlike micelles

At low concentrations, micelles generally have a spherical shape. However, in many micellar systems, micelles undergo a uni-axial growth into very long and flexible cylindrical micelles as the surfactant concentration is increased. Their size is determined by a balance between the scission energy required to create two end-caps where there were none before, and the entropy of mixing. Fig. 1 presents an example of the reduced dynamic viscoelastic spectra presented by two micellar solutions at different R values, 0.45 and 0.55, both measured for the same C_z = 46 mM and salt concentration (0.5 M in sodium chloride). At low frequencies, the elastic (storage) $G'(\omega)$ modulus and the viscous (loss) $G''(\omega)$ modulus follow approximately the expressions: $G' = G_0(\omega\tau)^2/[1+(\omega\tau)^2]$ and $G'' = G_0\omega\tau/[1+(\omega\tau)^2]$ typical of Maxwellian fluids, where G_0 is the elastic modulus at infinity frequency and τ is the relaxation time. Therefore, in both solutions, the stress relaxation function can be approximated by $G(t) = G_0\exp(-t/\tau)$. A stress relaxation dominated by a single exponential relaxation decay is considered a strong indication of the wormlike character of the self-assembled structures in the solution. Micelles, after growing and becoming wormlike, entangle above C* behaving in a similar way to polymers. However, in contrast to polymers, the size distribution of WMs is not quenched by synthesis; they break and recombine. The relaxation time is the geometric mean of two characteristic times, for micellar breaking and recombination, and for micellar reptation, as proposed by the reptation-reaction model [24]. The elastic moduli for the example of Fig. 1 are G_0 = 12 Pa for R = 0.55 and G_0 = 9.67 Pa for R = 0.45. Relaxation times are τ = 18.5 s for R = 0.55 and τ = 2.2 s for R = 0.45. Eliminating ω from the expressions of the moduli, the loss modulus can be expressed as a function of storage modulus (Cole–Cole plot) showing the form of a semicircle, as observed in an inset of Fig. 1 for both solutions. Shear induces birefringence in WM solutions because the supramolecular structures align under shear, producing birefringence. In an inset of Fig. 1, we also included a micellar solution (C_z = 46 mM, R = 0.45) disposed between two cross polarizers, with a stainless steel planar lab spatula dipping into the liquid. Prior to introducing the stainless steel spatula, the fluid is dark since light cannot pass through as in an isotropic fluid. However, as the spatula is introduced into the liquid, the fluid flows, as a result of the applied shear, and birefringence is clearly observed.

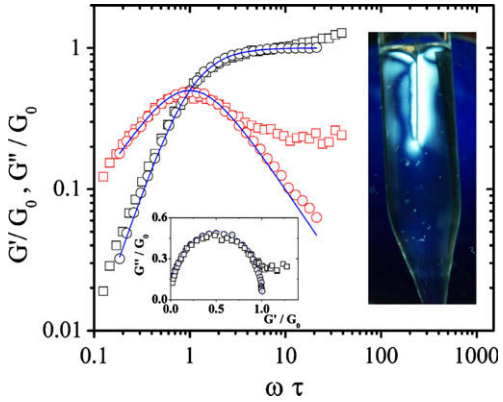

Fig. 1. An example of reduced dynamic viscoelastic spectra presented by this system for the case of R = 0.45 (□, G_0 = 9.7 Pa, τ = 2.2 s) and for R = 0.55 (○, G_0 = 12.0 Pa, τ = 18.5 s), both measured at the same C_z = 46 mM, salt concentration (0.5 M in sodium chloride), and T = 25 °C. Lines correspond to a Maxwell model fitting. Left inset: Cole–Cole diagram. Right inset: shear induced birefringence.

In Fig. 2, we present an example of HAADF TEM micrographs for air-dried WM samples (C_z = 2 mM, R = 0.55), negatively stained. HAADF is highly sensitive to variations in the atomic number of atoms in the sample, enabling us to obtain actual Z-contrast images of the micellar sample. In the micrograph, bright areas are enriched in uranium and dark areas (threadlike network) are depleted in that heavy metal. This is the place where the WM structures are located. Of course this technique is not absent of artifacts, related to solvent evaporation and uranyl acetate interaction. However in this case, micrographs showed very clearly an entangled net of long flexible tubular objects. The contour length of these objects exceeds several hundreds of nm and they have a diameter ~6 nm, close to the estimated length for two surfactants (~5 nm). The first conclusion of this work is that the system TDPS/SDS/brine self-assemble into long and flexible cylindrical micelles, i.e., WMs. As far as we know, this has not been reported before.

3.2. Dynamic light scattering and the overlap concentration

3.2.1. Intensity autocorrelation functions

Previous studies have reported that the intensity time correlation function becomes bimodal as the surfactant concentration is increased [25], in relative dilute WM solutions. This behavior helps to discriminate between two concentration regimes. At low surfactant concentrations, the fluid is made essentially of WMs that are relatively far apart, producing a fast mode due to the WM diffusion. At higher surfactant concentration, there is a slow mode that corresponds to structural relaxation of the network as a consequence of the WM entangling. In Fig. 3a and b, we present the intensity autocorrelation function for TDPS/SDS/water (0.5 M NaCl) for different C_z, at R = 0.45 and R = 0.55. At low C_z, there is just one mode of short relaxation time. As concentration increases, a slow mode of long relaxation time, albeit of very small amplitude, begins to evolve. As C_z increases, the fast mode relaxation time exhibits a monotonic decrease; however, the slow mode relaxation always increases. The slow mode becomes very prominent for $C_z \geqslant 30$ mM when R = 0.45, and for $C_z \geqslant 20$ mM when R = 0.55. The transition to

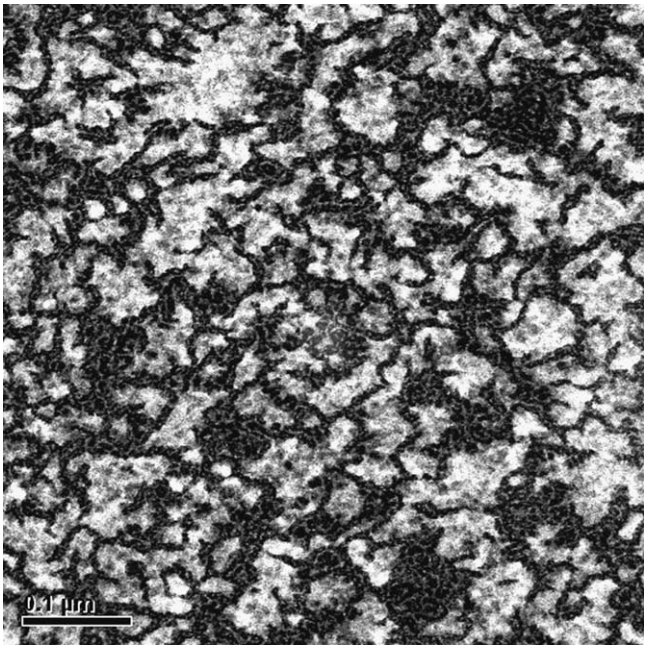

Fig. 2. HAADF TEM micrograph revealing an entangled net of long flexible tubular objects in the TDPS/SDS/water system negatively stained with uranyl acetate. Bright areas are enriched in uranium and dark areas (threadlike network) are depleted in that heavy metal, i.e., the place where WM are located.

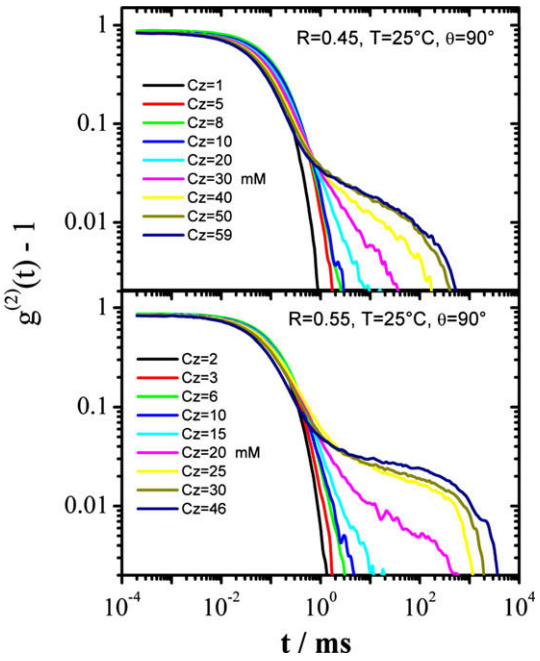

Fig. 3. Log–log intensity time autocorrelation function for the TDPS/SDS/water (0.5 M NaCl) system as a function of TDPS concentration (T = 25 °C). Upper panel R = 0.45 and lower panel R = 0.55.

the semidilute regime is defined by C^*, where WMs start to entangle with each other forming three dimensional transient networks. In our particular case, $C^* \sim 7$–8 mM for both R values. Many WM solutions present the same behavior when studied with DLS, as an example is the CTAB/NaSal/water system [25], where the overlap concentration is $C^* \sim 10$ mM, quite similar to the value found for our system.

3.2.2. Collective diffusion coefficient

DLS decay rates are linear functions of q^2 for the fast mode of the autocorrelation functions presented in Fig. 3a and b. From the slope of Γ vs q^2 lines, the collective diffusion coefficients were obtained and they are presented in Fig. 4. The micellar growth associated with the increase of zwitterionic surfactant concentration should produce a decrease in the diffusivity of the WMs, until a concentration around C^*, where WMs begin to overlap. Beyond this concentration, the time dependence of the concentration fluctuations is described by a cooperative diffusion mechanism [26]. As with ordinary polymer solutions, the corresponding D is independent of the lengths of the micelles, since the average micelle is large compared to the mesh size ξ. D is related to the hydrodynamic correlation length, ξ_H, through the Stokes–Einstein equation, and since ξ_H scales like ξ. Therefore, D should increase with surfactant concentration in the semidilute regime. This is exactly what was observed here. The values of C^* coming from the intensity autocorrelation functions agree well with the minima of the D *vs.* C_z curves ($C^* \sim 6$–7 mM) of Fig. 4.

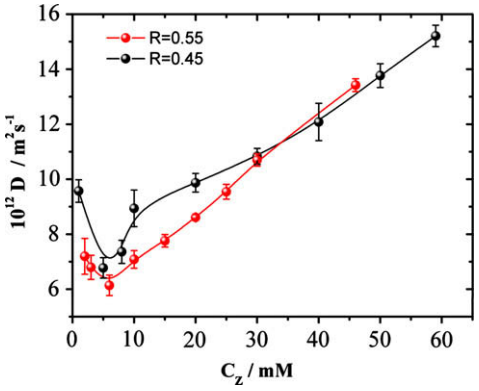

Fig. 4. Collective diffusion coefficient for different TDPS concentrations for R = 0.55 and R = 0.45. Lines are guides to the eye.

3.3. Rheological experiments for the WM solution at $C < C^*$

3.3.1. Thixotropic loops

In these experiments the shear rate is first ramped up (up-shear curve) from $\dot{\gamma} = 0$, to some maximum value and then it is ramped down (down-shear curve) at the same rate to $\dot{\gamma} = 0$. The shear rate sweeps used in this study are very small; always $\ddot{\gamma} \leqslant 0.5\ s^{-2}$. Fig. 5a presents the stress response during a thixotropic loop for a very dilute wormlike micellar solution (R = 0.55, C_z = 2 mM, and T = 25 °C). Shear stress increases almost linearly with $\dot{\gamma}$, until a critical shear rate $\dot{\gamma}_c$ is reached. From here, the shear stress increases in a nonlinear way until a regime where, again, the stress increases linearly with the shear rate. Within the experimental error limits, up-shear and down-shear curves can be superimposed. There is no hysteresis, as found recently in the C_nTAB surfactants [27]. Fig. 5b presents the apparent viscosity as a function of the applied shear rate for the up-shear curve of the thixotropic loop presented in Fig. 5a. Here, we observe three regimes similar to those described for others WM solutions [7,8,14,20,21]. In regime I, $\dot{\gamma} < \dot{\gamma}_c$, the viscosity is a few times greater than the viscosity of pure water or decreases slightly with the shear rate. In regime II, as $\dot{\gamma}$ increases above $\dot{\gamma}_c \sim 15\ s^{-1}$, the solution shear thickens until a maximum is reached at $\dot{\gamma} \sim 50\ s^{-1}$. In this particular case, viscosity increases by a factor of two, similar behavior has been observed in C_{14}TAB [23]. However, there are WM solutions where this factor is larger, as in the case of CTAB/NaSal in water [7,10,15], CTAT in water [8], TTAA/NaSal/isopropanol/H_2O [20], where viscosity increases by a

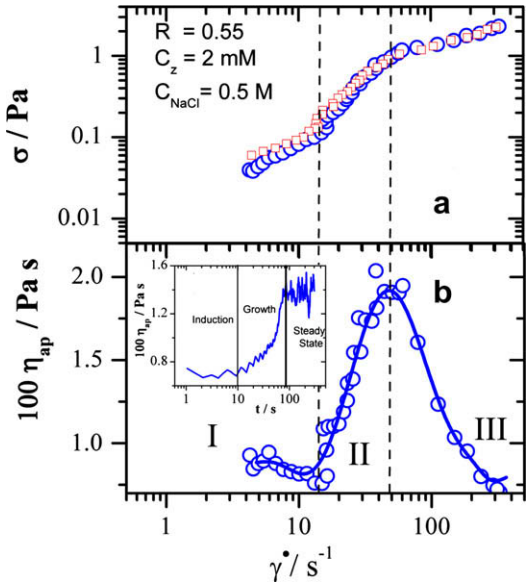

Fig. 5. Flow curves and viscosity for a WM solution with C_z = 2 mM, R = 0.55, and 25 °C. (a) Shear stress as a function of $\dot{\gamma}$ during a thixotropic loop for a very dilute micellar solution, using a small shear rate sweep (○; up-shear curve in blue, □; down-shear curve in red). (b) Apparent viscosity as a function of $\dot{\gamma}$ for the up-shear curve of the thixotropic loop presented in (a). The line is a guide to the eye. Inset: apparent viscosity as function of time for a step strain rate experiment at an imposed $\dot{\gamma} \sim \dot{\gamma}_c = 15\ s^{-1}$. (For interpretation of the references to colour in this figure legend, the reader is referred to the web version of this article.)

factor of 4, 20, and 4, respectively. The transition to this shear thickening regime is continuous. After that maximum, the solution shear thins defining the regime III. The WM solution also presents rheopexy as observed in step shear rate experiments. In step strain rate experiments close to $\dot{\gamma}_c$, at very low surfactant concentration (C_z = 2 mM) induction times are large, i.e., viscosity begins to increase after an induction period of 10 s, and it takes to the system ~100 s to reach the steady viscosity (inset of Fig. 5b). For the case of 2 mM and R = 0.45, the induction time is ~50 s. The induction time in this system decreases rapidly as surfactant concentration increases, up to the point that it is negligible after 5 mM. The shear thickening and the induction time has been interpreted as the time needed by the SIS to be formed [20,28]. We will come back to this issue below. This shear thickening behavior has not been observed before [11].

The different regimes mentioned above can also be observed in Fig. 6, where we present flow curves made by steadily increasing the level of applied shear stress, or by steadily increasing the level of applied shear rate in a WM solution with C_z = 5 mM. Regime I, occurs at low shear stress (below $\sigma_c \sim 0.36$ Pa) and shear rates (below $\dot{\gamma}_c \sim 50\ s^{-1}$). Here, the fluid is not much different from the equilibrium solution of WM micelles, with the exception that micelles probably tend to align with the imposed direction of shear flow. Regime II occurs along an intermediate range of stresses $\sigma_c < \sigma < \sigma_s \sim 2.2$ Pa. It is observed in steady state only under conditions of controlled shear stress. The steady state here is distinctive, because the shear rate first decreases as the stress increases above σ_c, and then once again $\dot{\gamma}$ increases when the shear stress is further increased. This behavior is similar to that presented by TTAA/NaSal/ isopropanol/H_2O [20]. It is important to mention that the points under shear stress control have an important error in the shear rate axis (~10%, not shown) along the gap defined by $\sigma_c < \sigma < \sigma_s$. Also in this gap, when the applied shear rate is steadily increased, some transient points can be captured. In this particular case, we captured a couple of points there. We also made shear inception experiments under shear stress control, and under shear rate control. These experiments closely follow the flow curves performed when shear stress or shear rate is steadily increased. Regime III occurs above a shear stress σ_s and above the shear rate $\dot{\gamma}_c$. Under conditions of controlled shear rate, the steady state behavior passed directly from regime I to regime III.

The effect of the C_z on viscosity can be observed in Fig. 7 for R = 0.45. Viscosities were obtained from the up-shear curves performed using very small shear rate sweeps ($\leqslant 0.3\ s^{-2}$), at 25 °C. The behavior of viscosity as a function of the shear rate is relatively similar for both R = 0.45 and R = 0.55 (not shown) values. In general, shear thickening moves to higher $\dot{\gamma}$ as C_z increases. This $\dot{\gamma}_c$ and the position of maximum viscosity reached during the thickening also increases with C_z. The shear thickening regime is less pronounced as C_z increases, and eventually it disappears after C^* is reached. This behavior is similar in other systems like in CTAT/D_2O [8], and TTAA/NaSal/ isopropanol/H_2O [20]. On the contrary, $\dot{\gamma}_c$ decreases with concentration in C_{14}DMAO/SDS [29], and Gemini 12-2-12 surfactant [30]. Before $\dot{\gamma}_c$, the system is Newtonian or slightly thinning for most of the cases of R = 0.45. At very low concentrations, the apparent viscosity, at low shear rates, is close to the solvent viscosity; the case of 2 mM is a clear example of this. For R = 0.55 in most of the cases, the micellar solutions are strongly thinning at low shear rates. This behavior, which is more pronounced here than for R = 0.45, reveals that at those concentrations the micelle shape has changed from nearly a spherical symmetry to an asymmetrical shape, which is sensitive to the orientating action of the velocity field. A similar thinning behavior has been observed in different systems as in CTAT/H_2O [8] and TTAA/NaSal/isopropanol/H_2O [20]. It is important to note that viscosity must start to increase appreciably at surfactant concentrations of the order of C^*, because of WM entanglement. This occurs for both R values around C_z = 8 mM. This value agrees well with C^* value obtained from DLS experiments. These values are of the same order of those in WMs made of CTAB and NaSal [7,10]. The inset of Fig. 7 presents how $\dot{\gamma}_c$ depends on C_z, at 25 °C for both R values. Here, it is interesting to note that addition of SDS to the micellar solution, when the R value is modified from R = 0.45 to 0.55, increases the value of $\dot{\gamma}_c$, that is, a larger shear rate is necessary to trigger the shear thickening when WMs are more charged.

The temperature dependence of the flow curves for the WM solutions under study was also investigated, for the two R values and C_z = 8 mM. At this C_z, although, the micellar solution is in the dilute regime limit, entangling is not important, however temperature effects are larger than in more dilute solutions. Flow curves were performed by steadily increasing the level of shear rate, with a slow sweep ramp ($\leqslant 0.3\ s^{-2}$). For both R values, we observed that the amount of shear thickening decreases as temperature increases. $\dot{\gamma}_c$ also increases with temperature, although, the change is more dramatic for the case of R = 0.55. In Fig. 8, we present a semilog diagram of the measured $\dot{\gamma}_c$ *vs* $1/T$ showing that the critical shear rate follows Arrhenius' law. The activation energy, E_a, is $E_a \sim 85$ kJ mol^{-1} for R = 0.45, and $E_a \sim 125$ kJ mol^{-1} for R = 0.55.

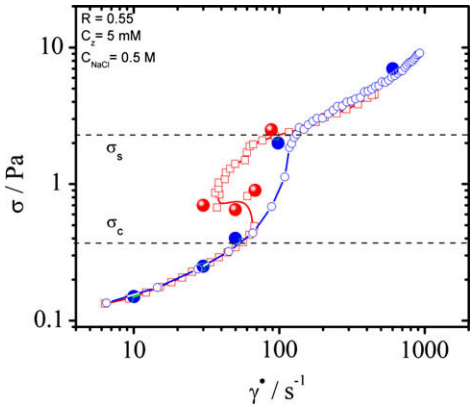

Fig. 6. Flow curves made by steadily increasing the level of applied shear stress (□) or by steadily increasing the level of applied shear rate (○). Solid points correspond to shear inception experiments in shear rate control (●), or in shear stress control (●). T = 25 °C. Lines are guides to the eye.

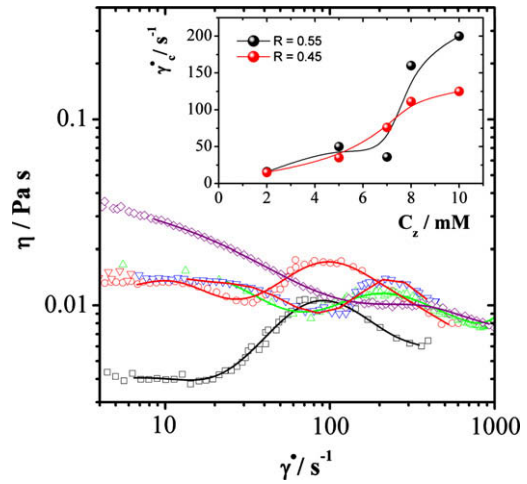

Fig. 7. Apparent viscosity as a function of C_z (2 □, 5 ○, 7 △, 8 ▽, and 10 ◇ mM), at R = 0.45, obtained from up-shear curves (T = 25 °C). Inset: $\dot{\gamma}_c$ vs. C_z for two R values. Lines are guides to the eye.

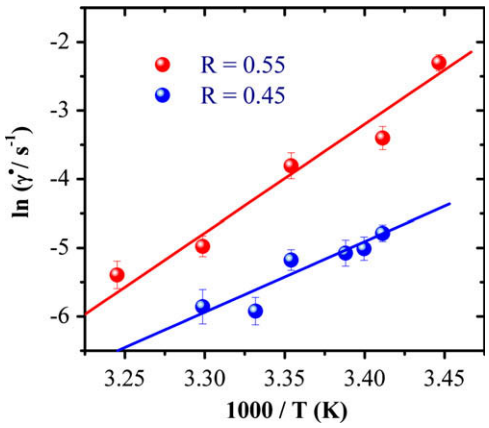

Fig. 8. $\dot{\gamma}_c$ as a function of $1/T$ and best fit lines for $R = 0.45$ and $R = 0.55$.

These values are smaller than the activation energies for the CTAT/D_2O system ($E_a \sim 306$ kJ/mol) [8], and of the same order of the EHAC/water (KCl) system, which ranges from 92.46 to 195.13 kJ/mol depending on the KCl concentration [17].

3.4. Observation of the shear-induced structures for the WM solution at $C < C*$

In Fig. 9, we present images of the scattered light from a sheet of light perpendicular to the flow, which is installed in the gap of a transparent Couette cell filled with the dilute micellar fluid ($R = 0.55$, $C_z = 2$ mM, $C_{NaCl} = 0.5$ M, $T = 25$ °C), which is under shear during a thixotropic loop. These images provide a direct evidence of the SIS formation. Observation of SIS is not common, they have been observed in CTAB/NaSal [7,22] in water and in TTAA/NaSal/isopropanol/H_2O [20,21]. Scattered light from the sheet of light reveals fluctuations in the dielectric constant due to fluctuations in density and in the nematic order parameter. Images for the ramping up process are presented in the lower part of the figure. The scattered light from the fluid is homogeneous along the observation window from $\dot{\gamma} = 0$ until the system reaches $\dot{\gamma}_c \sim 15\ s^{-1}$. This shear rate range corresponds approximately to regime I. When the system reaches $\dot{\gamma}_c$, at the beginning of the sigmoidal part of the curve, the system presents the formation of irregular bright and dark bands. The bright bands correspond to the SIS [7], and the dark bands to unstructured fluid. The bright bands become brighter and more defined as the fluid reaches regime III. In recorded films from the scattering experiments, these bands look like fluctuating. For an observer perpendicular to the sheet of light, these bands are neither fully aligned with the flow nor forming stationary structures along the Couette gap. However, they are statistically more aligned in the vertical direction, as if they were part of vertical inhomogeneous thick sheets parallel to the flow and coming to the observer along the flow direction. These vertical sheets separated by the unstructured fluid never form two separated blocks or regions in the fluid. The images during the ramping down process are shown in the upper part of Fig. 9. When the shear rate is along the down-shear curve, the SIS can be clearly observed in the gap, until the critical shear rate is reached. Here, the SIS disappear. This confirms that the system does not present hysteresis. This behavior is different from other systems like CTAB/NaSal/water [15], where SIS are delayed during the down shear process, and they remain visible practically until $\dot{\gamma} = 0$ [22].

4. Conclusions

We have acquired a new insight about structure and rheology of the TDPS/SDS/brine system not known before. First, this system self-assembles into long and flexible cylindrical micelles. Second, the main features of rheological behavior of this WM solution in the dilute regime (below the overlap concentration) were explored and compared with other WM solutions. The main results are: The

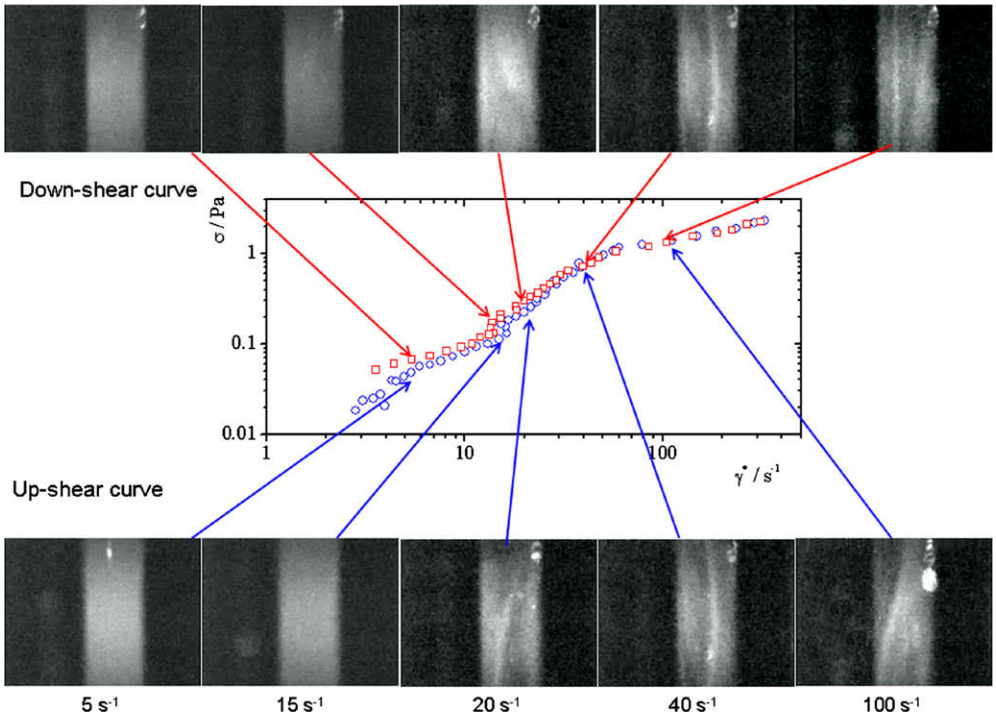

Fig. 9. Images of the scattered light from a sheet of light perpendicular to the flow, which is installed in the gap of a transparent Couette cell filled with a dilute micellar fluid which is under shear during a thixotropic loop ($R = 0.55$, $C_z = 2$ mM, $C_{NaCl} = 0.5$ M, $T = 25$ °C). Up-shear curve in blue and down-shear curve in red. (For interpretation of the references to colour in this figure legend, the reader is referred to the web version of this article.)

overlap concentration was determined (~7–8 mM), using the field autocorrelation functions obtained from DLS, and from the behavior of the collective diffusion vs. zwitterionic concentration. The behavior of the apparent viscosity and of the shear stress was determined, both as a function of the shear rate for different zwitterionic concentrations and temperatures, at two surfactant ratios ($R = [SDS]/[TDPS]$). The system presents a shear-thickening transition, where the critical shear rate increases as the zwitterionic concentration increases. We found that critical shear rate follows Arrhenius' law and activation energies were obtained. Finally, this is one of the very few systems where observations of shear-induced structures has been made in the dilute regime.

Our results help to understand the behavior of mixtures of zwitterionic and anionic surfactants that are employed in products for personal care and for household cleaning, because they are mild to skin and eyes, and easily biodegradable.

Acknowledgments

Funds from SEP-CONACYT (81081) and DGAPA-UNAM (112508) are gratefully acknowledged. We also thank to G. Jimenez for her help in DLS and to R. Hernandez for his technical support in TEM.

References

[1] K.D. Danov, S.D. Kralchevska, P.A. Kralchevsky, K.P. Ananthapadmanabhan, A. Lips, Langmuir 20 (2004) 5445.
[2] D. López-Díaz, I. García-Mateos, M.M. Velázquez, Colloids Surf. A 270–271 (2006) 153.
[3] C.A. Dreiss, Soft Matter 3 (2007) 956.
[4] D.P. Acharya, H. Kunieda, Adv. Colloid Interface Sci. 123–126 (2006) 401.
[5] J.F Berret, Rheology of wormlike micelles: equilibrium properties and shear banding transitions, in: R.G. Weiss, P. Terech (Eds.), Molecular Gels. Materials with Self-Assembled Fibrillar Networks, Springer, The Netherlands, 2006, pp. 663–715.
[6] L.M. Walker, Curr. Opinion Colloid Interface Sci. 6 (2001) 451.
[7] C. Liu, D.J. Pine, Phys. Rev. Lett. 77 (1996) 2121.
[8] R. Gamez-Corrales, J.F. Berret, L.M. Walker, J. Oberdisse, Langmuir 15 (1999) 6755.
[9] J.F. Berret, R. Gámez-Corrales, J. Oberdisse, L.M. Walker, P. Lindner, Europhys. Lett. 41 (1998) 677.
[10] H. Hu, S.Q. Wang, A.M. Jamieson, J. Rheol. 37 (1993) 531.
[11] S. Lerouge, J. F. Berret, Adv. Polym. Sci. doi:10.1007/12200913.
[12] U.R.K. Rao, C. Manohar, B.S. Valaulikar, R.M. Iyer, J. Phys. Chem. 91 (1987) 3286.
[13] J.F. Berret, R. Gámez-Corrales, Y. Séréro, F. Molino, P. Lindner, Europhys. Lett. 54 (2001) 605.
[14] J.F. Berret, R. Gámez-Corrales, S. Lerouge, J.P. Decruppe, Eur. Phys. J. E 2 (2000) 343.
[15] P. Ballesta, S. Manneville, Europhys. Lett. 76 (2006) 429.
[16] Y. Hu, C.V. Rajaram, S.Q. Wang, A.M. Jamieson, Langmuir 10 (1994) 80.
[17] V. Groce, T. Cosgrove, G. Maitland, T. Hughes, G. Karlsson, Langmuir 19 (2003) 8536.
[18] H. Hu, R.G. Larson, J.J. Magda, J. Rheol. 46 (2002) 1001.
[19] R. Oda, V. Weber, P. Lindner, D.J. Pine, E. Mendes, F. Schosseler, Langmuir 16 (2000) 4859.
[20] Y.T. Hu, P. Boltenhagen, D.J. Pine, J. Rheol. 42 (1998) 1185.
[21] Y.T. Hu, P. Boltenhagen, E. Matthys, D.J. Pine, J. Rheol. 42 (1998) 1209.
[22] J. Delgado, R. Castillo, J. Colloid Interface Sci. 312 (2007) 481.
[23] J. Dehmoune, J.P. Decruppe, O. Greffier, H. Xu, P. Lindner, Langmuir 25 (2009) 7271.
[24] M.E. Cates, Macromolecules 20 (1987) 2289.
[25] S. Amin, T.W. Kermis, R.M. van Zanten, S.J. Dees, J.H. van Zanten, Langmuir 17 (2001) 8055.
[26] P.-G. de Genes, Scaling Concepts in Polymer Physics, Cornell University Press, Ithaca, 1979.
[27] J. Dehmoune, J.P. Decruppe, O. Greffier, H. Xu, J. Rheol. 52 (2008) 923.
[28] J.F. Berret, S. Lerouge, J.P. Decruppe, Langmuir 18 (2002) 7279.
[29] S. Hofmann, A. Rauscher, H. Hofmann, Phys. Chem. 95 (1991) 153.
[30] R. Oda, P. Panizzza, M. Schmutz, F. Lequeux, Langmuir 13 (1997) 6407.